Volume 24, No 3 | International Journal of Radiation Research, July 2026

Prediction of treatment response in inoperable cervical cancer treated with curative radiotherapy using artificial intelligence with radiomic and clinical parameters

M. Yakar[1*], D. Etiz[1], K. Duruer[1], E. Gulbandilar[2], E. Colak[3], B. Barut[1]

[1]*Department of Radiation Oncology, Faculty of Medicine, Osmangazi University, Eskişehir, Turkey*
[2]*Department of Computer Engineering, Faculty of Engineering, Osmangazi University, Eskişehir, Turkey*
[3]*Department of Biostatistics, Faculty of Medicine, Osmangazi University, Eskişehir, Turkey*

► ***Original article***

Corresponding author:
Melek Yakar, Ph.D.,
E-mail: *myakar@ogu.edu.tr*

Received: December 2024
Final revised: October 2025
Accepted: December 2025

Int. J. Radiat. Res., July 2026; 24(3): 647-654

DOI: 10.61186/ijrr.24.3.9

Keywords: *Uterine cervical neoplasms, radiomics, radiotherapy, chemoradiotherapy, prognosis, image processing - computer assisted.*

ABSTRACT

Background: Radiomic features extracted from the tumor and peritumoral region can be used to predict response to radiotherapy (RT). This research sought to estimate treatment response through the analysis of tumor and peritumoral radiomic features in patients receiving curative radiotherapy for cervical cancer. ***Materials and Methods:*** Between 2015 and 2024, 60 patients with cervical cancer who underwent radiotherapy (RT) with or without chemotherapy (ChT) were included in the study Tumor segmentation was performed using computed tomography (CT) scans. Radiomic feature extraction was carried out with the LifeX platform (v7.0.0). A total of 110 tumoral and peritumoral radiomic features were obtained. 19 clinical and 110 radiomic features were evaluated, and important variables were identified using a decision tree algorithm. Treatment response following RT was evaluated based on the RECIST guidelines. The k-Nearest Neighbors (kNN) and Multi-Layer Perceptron (MLP) algorithms were used to build a prediction model. ***Results:*** The analysis identified total EQD2, EBRT interruption time, peritumoral_GLZLM_ZLNU, GTV_GLZLM_ZLNU, and GTV_GLRLM_LRLGE as significant predictive variables. Among the predictive algorithms developed for key variables, the k-Nearest Neighbors (kNN) model achieved F1 scores of 0.84 and 0.74 on the training and testing datasets, respectively, while the Multi-Layer Perceptron (MLP) model achieved F1 scores of 0.96 and 0.81 on the training and testing datasets, respectively. ***Conclusion:*** Non-invasive, tumor-signature radiomics show promise for guiding personalized therapies. The radiomic parameters Peritumoral_GLZLM_ZLNU, GTV_GLZLM_ZLNU, and GTV_GLRLM_LRLGE emerged as key predictors of treatment response to radiotherapy. Nevertheless, further multicenter research involving larger patient cohorts is required to achieve more robust and generalizable results.

INTRODUCTION

Globally, cervical cancer ranks among the leading malignancies in women, particularly in those of reproductive age [(1)]. Approximately 95% of cervical cancer cases are attributed to infection with the human papillomavirus (HPV) [(2)]. The prevalence of chronic HPV infection is estimated to be around 10-20% in regions where cervical cancer is common, while it decreases to approximately 5-10% in areas with lower disease incidence [(3)]. The cervix is an ideal site for cancer screening due to its anatomical accessibility for examination and the long interval between initial DNA damage and the development of invasive cancer.

Recent decades have witnessed improved survival in cervical cancer due to the implementation of organized screening and advancements in radiotherapy technologies. Regardless of cancer histopathology or HPV infection status, primary curative treatment in cervical cancer patients usually consists of surgery, chemoradiotherapy (CRT), or a combination of these modalities, with treatment options varying by cancer stage.

Treatment approaches vary depending on a patient's condition and cancer stage but generally include a combination of external beam radiotherapy (EBRT), concurrent chemotherapy (CBT), and brachytherapy (BRT). While treatments are standardized according to disease stage, the same oncological outcomes are not always achieved in patients at the same stage. This lack of consistent response to standard therapy highlights the importance of personalized treatments and the many other parameters that can influence individual treatment decisions. Features obtained from imaging methods such as radiomics can guide clinicians in personalized treatment approaches. Radiomics are quantitative features derived from medical imaging data through advanced mathematical analysis [(4)].

Radiomics contains quantitative data that cannot be detected by the human eye. This quantitative data contains tumor-specific characteristics [5].

Recent studies highlight that the characteristics of the surrounding tissue, in addition to those of the tumor itself, play an important role in influencing tumor progression and therapeutic response.Specifically, peritumoral radiomics enables the extraction of biological and physical properties from the surrounding tissue. These techniques enable a better understanding of how the tumor microenvironment influences tumor growth and metastatic potential. The radiomic features obtained from this region can therefore be used to predict tumor aggressiveness and response to RT with greater accuracy [6, 7].

This study evaluated the potential of tumor and peritumoral radiomics to predict treatment response in patients with cervical cancer undergoing definitive radiotherapy (RT) with or without chemotherapy (ChT).

MATERIALS AND METHODS

Patients

A total of 60 patients receiving curative radiotherapy, with or without concurrent chemotherapy, between 2015 and 2024 were enrolled in the study. Patients eligible for inclusion were 18 years of age or older and had histologically confirmed cervical carcinoma, classified as locally advanced based on clinical or radiological evaluation. Individuals were excluded if they had poor performance status (KPS <60), distant metastases, incomplete therapy, or irregular follow-up. Ethical approval for this study was obtained from the Non-Interventional Clinical Research Ethics Committee of Eskişehir Osmangazi University (Approval No: E-25403353-050.04-240226745; dated 28 November 2024).

Treatment

CT-based simulation was performed with the patient in supine position using non-contrast images encompassing the pelvis at 2–5 mm slice thickness. Planning CT scans were acquired for all patients with a full bladder and empty rectum using a Discovery RT CT device (General Electric, United States) at 120 kVp. Two-dimensional bladder measurements were performed using a SonoStar wireless probe-type ultrasound scanner (Guangzhou, China) prior to planning CT. Planning CT images, along with additional imaging modalities such as magnetic resonance imaging (MRI; Siemens Magnetom Avanto TIM MR, Germany) or fluorodeoxyglucose positron emission tomography/computed tomography (FDG-PET/CT; Siemens Biograph Vision 450 Digital PET/BT, Germany), were used to contour the tumor and surrounding critical structures accurately. Target volumes (GTV, CTV, and PTV) and organs at risk - including rectum, bladder, bowel, and femoral heads - were delineated in accordance with international contouring standards [8-9]. The peritumoral area surrounding the tumor was also contoured for the study. Patients' treatment planning was performed using intensity modulated radiotherapy (IMRT) or volumetric modulated arc therapy (VMAT) techniques (figure 1a). Patients were treated with Varian TrueBeam® or Varian Trilogy® (Palo Alto, United States) devices. In the treatment plan, attention was paid to protecting OAR while ensuring adequate dose delivery to the target volume. EBRT was delivered at 40-50.4 Gy (1.8-2 Gy/day) followed by an additional 10-15 Gy boost to pathological lymph nodes, with OAR dose constraints taken into account. BRT planning was performed in 3D and delivered with Varian GammaMed Plus iX® device (Palo Alto, United States) with Ir-192 radioactive source at doses of 16.5-30 Gy/2-5 fr. Weekly cisplatin (40 mg/m^2) was administered concurrently, with dosing guided by patient condition, Karnofsky Performance Status (KPS), laboratory values, and comorbidities. During the treatment period, patients were followed up in the outpatient setting at least once per week. For this study, peritumoral radiomic contours were created as GTV + 3mm, with the GTV itself excluded; radiomic features were then extracted from the remaining peritumoral ring (figure 1b).

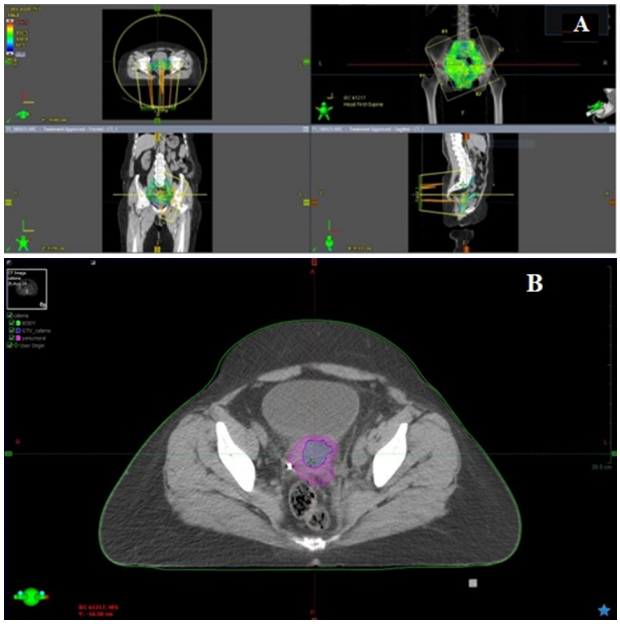


Figure 1. (A) Dose distribution map from radiotherapy planning in a patient with cervical cancer, illustrating target coverage. **(B)** Segmentation of target and peritumoral ROI' s used for feature extraction.

Follow-Up

Follow-up evaluations were scheduled quarterly during the first two years, semiannually up to the fifth year, and once a year thereafter. Response assessments were performed using pelvic MRI and

FDG-PET CT at 3-6 months after completion of treatment. Any patients with suspected recurrence or residual disease were then evaluated by a multidisciplinary Gynecology-Oncology council. Response assessment to treatment was performed according to the Response Evaluation Criteria in Solid Tumors (RECIST) and metabolic response in FDG PET CT.

Extraction of radiomic features

Radiomic data were extracted from the planning CT datasets used in RT simulation at the Department of Radiation Oncology, Eskişehir Osmangazi University Faculty of Medicine. All images were obtained using the same CT scanner and standardized imaging protocol. GTV and peritumoral regions of interest (ROIs) were delineated in the Varian Eclipse radiotherapy treatment planning system (Version 15.6, Palo Alto, United States). Feature computation was conducted via LifeX software (v7.0.0, Inserm, France), applying a 1×1×1 mm spatial resampling grid and a 32-bin discretization scheme. Based on these predefined parameters, three-dimensional (3D) image processing was conducted, yielding 55 radiomic features for each ROI (table 1).

Table 1. First and second order radiomics.

First Order	CONVENTIONAL_HUmin, CONVENTIONAL_HUmean, CONVENTIONAL_HUstd, CONVENTIONAL_Humax, CONVENTIONAL_HUSkewness, CONVENTIONAL_HUKurtosis, CONVENTIONAL_HUExcessKurtosis, DISCRETIZED_HUmin, DISCRETIZED_HUmean, DISCRETIZED_HUstd, DISCRETIZED_HUmax, DISCRETIZED_HUSkewness, DISCRETIZED_HUKurtosis, DISCRETIZED_HUExcessKurtosis, DISCRETIZED_HISTO_Entropy_log10, DISCRETIZED_HISTO_Entropy_log2, DISCRETIZED_HISTO_Energy, DISCRETIZED_AUC_CSH, SHAPE_Volume (mL), SHAPE_Volume (vx), SHAPE_Sphericity, SHAPE_Surface (mm^2), SHAPE_Compacity
Second Order	GLCM_Homogeneity, GLCM_Energy, GLCM_Contrast, GLCM_Correlation, GLCM_Entropy_log10, GLCM_Entropy_log2,GLCM_Dissimilarity, GLRLM_SRE, GLRLM_LRE, GLRLM_LGRE, GLRLM_HGRE, GLRLM_SRLGE, GLRLM_SRHGE, GLRLM_LRLGE, GLRLM_LRHGE, GLRLM_GLNU, GLRLM_RLNU, GLRLM_RP, NGLDM_Coarseness, NGLDM_Contrast, NGLDM_Busyness, GLZLM_SZE, GLZLM_LZE, GLZLM_LGZE, GLZLM_HGZE, GLZLM_SZLGE, GLZLM_SZHGE, GLZLM_LZLGE, GLZLM_LZHGE, GLZLM_GLNU, GLZLM_ZLNU, GLZLM_ZP

Clinical parameters

In addition to GTV and peritumoral radiomics, clinical parameters were also incorporated into the modeling. The clinical parameters evaluated included: age, KPS, presence of diabetes mellitus, histopathology, presence of radiologically pathological lymph nodes, Tumor- Node- Metastasis (TNM) stage, largest tumor diameter, presence of adjacent organ invasion, pre- and post-RT CA-125 levels, GTV, PTV, lowest hemoglobin level during RT, EBRT dose, EBRT interruptions, presence of BRT, BRT dose, total equivalent dose in 2 Gy fractions (EQD2), and concurrent ChT.

Statistical analysis and artificial intelligence

Radiomics feature selection

The dataset comprised 129 features extracted from 60 patients. The target variable was binary, classified as “complete response to treatment” versus “no complete response to treatment (partial or stable responses).” To address data imbalance, oversampling of minority cases was implemented through the the Synthetic Minority Oversampling Technique(SMOTE) algorithm within Python [10], increasing the dataset to 80 samples.

Feature importance was evaluated using a decision-tree approach designed to identify the parameters with highest predictive contribution. Tree-based models represent one of the most flexible supervised learning approaches, capable of addressing both classification and regression analyses effectively. In this analysis, the Gini index was applied as a criterion to quantify dataset impurity through probability-based evaluation of categorical variables. Once the feature providing the greatest information gain was designated as the root node, the algorithm iteratively refined the branching structure to enhance prediction performance. The analyses were performed using scikit-learn and the decision tree method. The model’s "accuracy rate" is defined as the proportion of correct predictions made. We also evaluated the accuracy rate for various feature subsets [11].

Artificial intelligence-based prediction algorithms

Five significant variables from the decision tree model were used as inputs, with treatment response as the output. The patient group, expanded to 80 patients using SMOTE, was employed for training and testing. Two different models were developed with this dataset to predict treatment response. For both models, 70% of the data were randomly assigned to training and the remaining 30% to testing.

In this study, two algorithms were applied. The first was the k-Nearest Neighbors (kNN) method, one of the most commonly used approaches in machine learning. The principle behind kNN is straightforward: when a new data point is introduced, the algorithm identifies the closest examples in the training set. For classification tasks, it assigns the most label frequent among these neighbors, whereas for regression tasks, it calculates their average value. To evaluate model performance, several metrics were considered, including accuracy, precision, recall, and the F1 score. The implementation was carried out in Python using the widely adopted scikit-learn library [12].

As a second method, a Multilayer Perceptron (MLP) model was applied to the same dataset. MLPs

are a type of deep learning model composed of layers of densely connected neurons. Each neuron passes information to the next layer, creating a network that can capture complex patterns in the data. In this study, the MLP architecture consisted of an input layer, two hidden layers, and a single output layer.The model was built and tested using Python libraries, alongside the earlier kNN implementation [12].

RESULTS

Patient characteristics and treatment outcomes

The median age of the study cohort was 56 years (range: 32–83), and the median KPS score was 70 (range: 60-90). The majority (85%) had squamous cell carcinoma, whereas adenocarcinoma accounted for 15%. Regarding staging, 35 (58.3%) patients had radiological pathological lymph node metastasis, and 7 (11.7%) had adjacent organ invasion. The median tumor's greatest diameter was 50 mm (min: 30, max: 140). The median GTV and PTV were 141 cc (min: 22, max: 789) and 315 cc (min: 54, max: 1069), respectively. During RT, the lowest observed hemoglobin value was a median of 9.7 g/dL (min: 5.9, max: 14.2). The median EBRT dose was 50.4 Gy (min: 45, max: 66.5). The median EQD2 value was 83 Gy (min: 44, max: 104), and the median CA-125 value was 18.6 U/mL before RT and 13.8 after RT. A total of 54 (90.0%) patients received concomitant cisplatin ChT. Following EBRT, 51 patients received BRT, 2 patients received boost with stereotactic body radiotherapy, and 7 patients did not receive boost due to patient refusal, a tumor size unsuitable for BRT after EBRT, or age or KPS.

Treatment response assessment revealed complete remission in 48 individuals (80%), partial remission in 11 (18%), and stable disease in one patient (2%). In the median follow-up period of 32 months, 42 patients were alive, and 18 patients had died. While 48 patients had no distant metastasis, 12 patients developed distant metastasis during follow-up. The median overall survival was 32 months (range: 5-102), and the median disease-free survival was 30.5 months (range: 1-100). Patient, tumor, and treatment characteristics are summarized in table 2.

Important clinical and radiomic features

In total, 110 radiomic descriptors were obtained, equally divided between the tumoral and peritumoral regions. The decision tree analysis identified several key predictors- namely *peritumoral Gray-Level Zone Length Matrix–Zone Length Non-Uniformity (GLZLM_ZLNU)*, *Gross Tumor Volume Gray-Level Zone Length Matrix–Zone Length Non-Uniformity (GTV_GLZLM_ZLNU)*, and *Gross Tumor Volume Gray-Level Run Length Matrix–Long-Run Low Gray-Level Emphasis(GTV_GLRLM_LRLGE)*- as the most influential parameters in forecasting treatment response.Additionally, from the 19 clinical variables, total EQD2 and the duration of interruption of EBRT were found to be important features. In order of importance (measured by entropy), the features were ranked as follows: total EQD2 (entropy: 1.0), duration of interruption of EBRT (entropy: 0.8), peritumoral_GLZLM_ZLNU (entropy: 0.6), GTV_GLRLM_LRLGE (entropy: 0.5), and GTV_GLZLM_ZLNU (entropy: 0.3). Using the dataset augmented by SMOTE, the resulting decision tree is illustrated in figure 2a. The model achieved an accuracy rate of 0.72 for the training set and 0.75 for the testing set. The graph of important variables is shown in figure 2b.

Table 2. Patient, Tumor and Treatment Characteristics.

Features	Number of patients (%)/ Median (min-max)
Age	56 (32-83)
KPS	70 (60-90)
Diabetes mellitus	
+	12 (20.0%)
-	48 (80.0%)
Histopathology	
Squamous cell carcinoma	51 (85.0%)
Adenocarcinoma	9 (15.0%)
Radiological lymph node metastasis	
+	25 (41.7%)
-	35 (58.3%)
TNM Stage	
IIA	2 (3.3%)
IIB	30 (50.0%)
IIIA	1 (1.7%)
IIIC	19 (31.7%)
IVA	8 (13.3%)
CA-125 (U/mL)	
Before RT	18.6 (3.1- 279.0)
After RT	13.8 (3.8- 90.3)
GTV (cc)	141 (22-789)
PTV (cc)	315 (54- 1069)
EBRT Dose (Gy)	50.4 (45- 62.5)
EBRT interruption time (days)	2(0-12)
Post-EBRT Boost	
+	53 (88.3%)
-	7 (11.6%)
Concurrent chemotherapy	
+	54 (90.0%)
-	6 (10.0%)
Total EQD2 (Gy)	83 (44-104)

Results of ai-based prediction algorithms

For the kNN classifier, accurate identification was achieved in 29 of 32 complete-response cases and 25 of 32 non-response cases in the training dataset. In the test group, the kNN algorithm correctly predicted 5 out of 8 cases with a CR and 7 out of 8 cases without a CR. The kNN model, developed with a Python-based framework, yielded the training and test results summarized in table 3.Model performance metrics, derived from these results, are likewise reported in the same table.The receiver operating characteristic (ROC) curves for both training and test datasets are illustrated in figures 3a and 3b.The MLP model demonstrated near-perfect accuracy, correctly classifying all complete responders and 30 of 32 non-

responders in the training dataset. In the test group, the MLP algorithm correctly predicted 6 out of 8 cases with a CR and 7 out of 8 cases without a CR. The MLP model, implemented through a Python-based environment, produced the training and test outcomes summarized in table 4. Corresponding model performance metrics, obtained from these results, are likewise reported in the same table. The receiver operating characteristic (ROC) curves for the training and test sets are depicted in figures 4a and 4b.

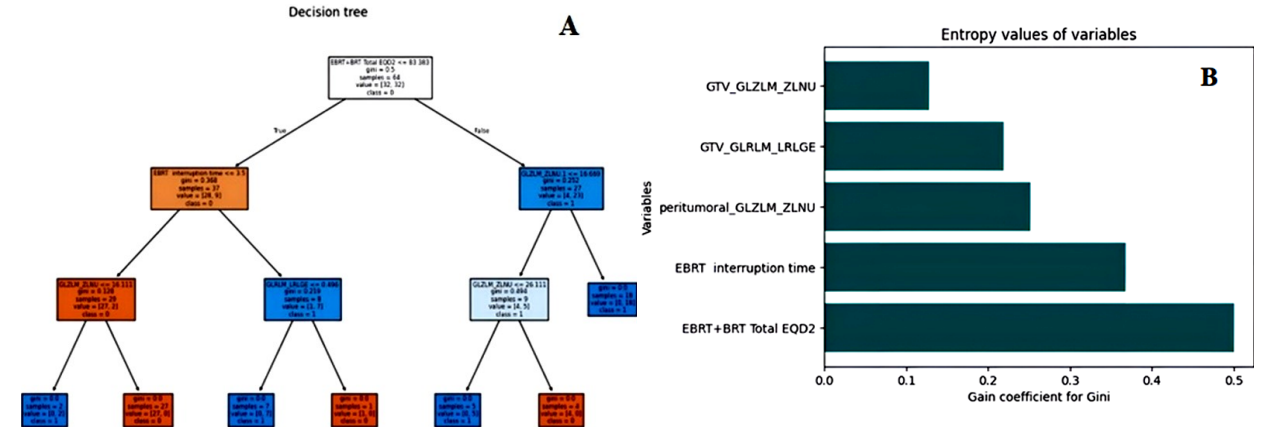


Figure 2. (A) This decision tree illustrates the classification of patients based on radiotherapy parameters (EBRT+BRT Total EQD2, EBRT interruption time, and texture features such as GLRLM_LRLGE and GLZLM_ZLNU). It demonstrates how treatment dose and radiomic features contribute to predicting patient outcomes (class 0 vs. class 1). **(B)** Graph of the most important variables contributing to the decision tree model, ranked according to their predictive value for treatment response. EBRT: external beam radiotherapy, BRT: brachytherapy, GLZLM_ZLNU: The grey-level zone length matrix_ Zone Length Non-Uniformity, GLRLM_LRLGE: The grey-level run length matrix_ Long-Run Low Gray-level Emphasis GTV: gross tumor volume.

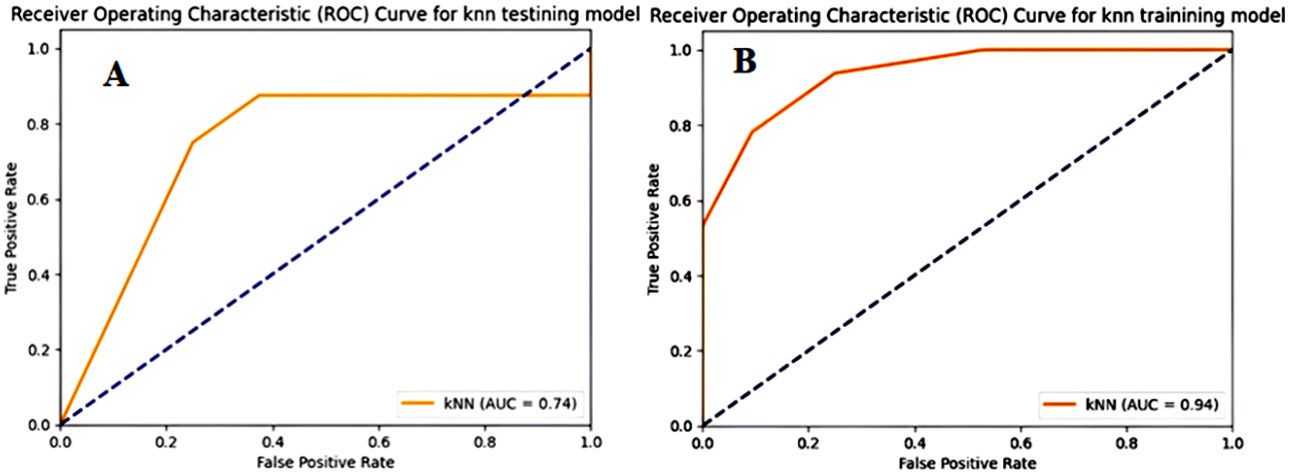


Figure 3. Receiver operating characteristic (ROC) curve of the k-Nearest Neighbors (kNN) algorithm on the training dataset, demonstrating the model's discrimination ability (A). ROC curve of the kNN algorithm on the test dataset, showing the predictive performance on unseen data (B).

Table 3. Confusion matrices for both the training and the test datasets, together with the corresponding performance metrics (accuracy, sensitivity, specificity, and AUC) of the k-Nearest Neighbor (kNN) classification algorithm. The table summarizes how well the model distinguished between responders and non-responders in both datasets.

Actual	CR	Train predicted		Test predicted	
		+	-	+	-
	+	29	3	5	3
	-	7	25	1	7
		Training		Test	
Accuracy		0.844		0.750	
Precision		0.849		0.767	
Recall		0.844		0.750	
F1 Score		0.843		0.746	

CR: Complete response

Table 4. Confusion matrices for both the training and the test datasets, together with the corresponding performance metrics (accuracy, sensitivity, specificity, and AUC) of the Multi -Layer Perceptron (MLP) classification algorithm. The table illustrates how effectively the model discriminated between responders and non-responders in both datasets.

Actual	CR	Training prediction		Test prediction	
		+	-	+	-
	+	32	0	6	2
	-	2	30	1	7
		Training prediction		Test prediction	
Accuracy		0.967		0.813	
Precision		0.971		0.818	
Recall		0.969		0.813	
F1 Score		0.969		0.812	

CR: Complete response

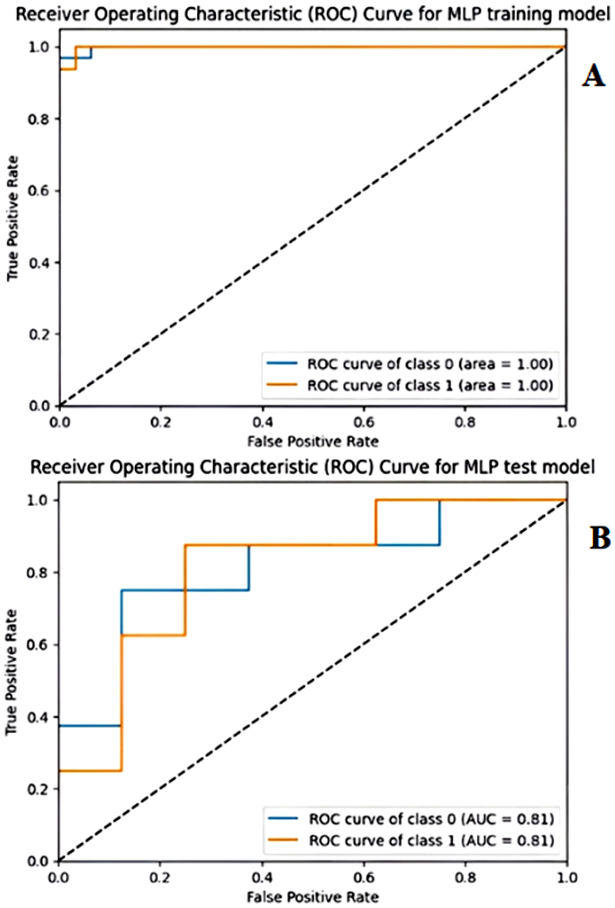


Figure 4. ROC curve of the Multi-Layer Perceptron (MLP) algorithm on the training dataset, illustrating the classification performance of the neural network model **(A)**. ROC curve of the MLP algorithm on the test dataset, demonstrating the generalizability and performance of the MLP model on independent data **(B)**.

DISCUSSION

Concurrent chemoradiation with platinum-based regimens remains the cornerstone of therapy for locally advanced cervical carcinoma, offering optimal local control and survival outcomes. Although this approach significantly improves locoregional control and overall survival, cancer recurs in up to 40% of patients [13]. Comparable oncological outcomes cannot be achieved with standard treatments in patients with the same clinical and pathological prognostic factors and disease stage. This difference may be attributed to tumor heterogeneity at the phenotypic and genotypic levels, which cannot be revealed through standard diagnostic methods. Medical imaging, however, contains far more information than the human eye can detect. This additional information can provide valuable insights into tumor characteristics. With advances in computer technology, numerous quantitative features – known as radiomics – can now be extracted from medical images. Artificial intelligence algorithms can be used in conjunction with radiomics to process this vast amount of data more effectively. Radiomic features, often referred to as tumor signatures, have the potential to support personalized cancer treatment. "Radiomics employs algorithmic techniques to quantify textural and structural characteristics within medical images, providing a computational representation of tumor biology [14]. Quantitative features extracted from imaging data frequently mirror the intrinsic biological traits of the tumor [15]. Consequently, tumor behavior, as well as sensitivity or resistance to radiation therapy, may be predicted using radiomics. The peritumoral interface, where neoplastic and normal tissues interact, exhibits pronounced biological and structural alterations throughout tumor evolution and therapeutic response. This interface functions as a dynamic niche mediating immune modulation, cellular signaling, and extracellular remodeling processes that influence tumor behavior [16].

Radiomics features such as GLZLM (Gray-Level Region Length Matrix) and GLRLM (Gray-Level Run Length Matrix) are widely used to capture and quantify tissue heterogeneity in medical images. GLZLM evaluates the uniformity or diversity of tissue structure by analyzing the lengths of regions with similar grayscale values. One of its metrics, GLZLM_ZLNU, measures the irregularity of grayscale region lengths, with greater irregularity generally indicating higher tissue heterogeneity.

GLRLM analyzes the lengths of consecutive regions of similar grayscale values within an image. This matrix characterizes tissue heterogeneity by quantifying sequences of adjacent gray-level runs of varying lengths within the image structure.The GLRLM_LRLGE radiomics feature specifically captures regions with low grayscale values. In the field of oncology, radiomics is an important tool for predicting tumor response to treatment because these features reflect the underlying heterogeneity of tumor tissue. In cervical cancer, radiomics analyses can help in selecting patient-specific treatments and making prognostic assessments. For example, higher ZLNU values might suggest that the tumor tissue is more heterogeneous and, consequently, may respond less effectively to RT. Similarly, analyzing LRLGE values can provide insights into how specific regions of the tumor with low gray-level features might respond to treatment [17-18].

Tumor heterogeneity can explain why different tumor cells respond differently to radiotherapy and other cancer treatments. This heterogeneity may arise from molecular differences in cancer stem cells [19]. In addition, areas of necrosis within a tumor can also contribute to tissue heterogeneity. Necrotic tumors are known to be resistant to RT, primarily due to inadequate oxygenation. Therefore, the presence of both RT-resistant stem cells and necrosis may contribute to overall RT resistance by increasing

tissue heterogeneity.

In a study by Jha *et al.*, machine learning techniques were used to predict survival in 68 patients with advanced cervical cancer treated with CRT, utilizing clinical and CT radiomic features. Their logistic regression algorithm, which incorporated both radiomic and hybrid (clinical + radiomic) features, achieved a survival prediction accuracy of 69%. Consistent with our findings, their analysis also highlighted GLRLM as a major radiomic feature of predictive importance [20]. This aligns with our approach, which also employed a hybrid model combining both clinical and radiomic features.

A study conducted by Lucia *et al.* evaluated PET and MRI radiomics in 102 cervical cancer patients. Consistent with our findings, they determined that GLRLM radiomics was a more effective prognostic factor than clinical parameters [21]. Their model achieved a recurrence prediction accuracy of 94%. The elevated accuracy observed in their analysis could be explained by the inclusion of a broader and more diverse patient cohort, supporting our assumption that model performance tends to improve with larger and heterogeneous populations. Similarly, in a study of 44 patients with FIGO stage IB2-Iva cervical cancer, Leseur *et al.* evaluated 22 radiomic features from PET images. They found that GLRLM_GLNU and GLRLM_RLNU radiomics were significantly associated with OS [22]. This study also reinforces the importance of GLRLM radiomics, much like our own research.

Studies using MRI radiomics have shown that GLZLM features can predict disease-free survival, overall survival, progression-free survival, and treatment response in cervical cancer patients, with AUCs ranging from 0.78 to 0.91 [23-25]. The use of MRI is advantageous because it can more precisely define tumor location. However, our study utilized CT images for RT planning. It is important that the imaging modality used for extracting radiomic features in cervical cancer studies be standardized. Similar to our findings, GLZLM demonstrated significant prognostic value in these studies. Furthermore, Ho *et al.* found that GLRLM_GLNU measured before CRT and GLSZM_ΔGLNU two weeks after CRT could differentiate between patients who achieved a complete metabolic response and those who did not (AUC 0.76-0.77) [26]. This finding, like ours, highlights the prognostic potential of GLRLM features.

For increased local control, a total EQD2 dose of ≥ 80 Gy is recommended for tumors that show a complete or partial response after EBRT and that have a residual size smaller than 4 cm. For non-responding tumors or residual tumors larger than 4 cm, a total EQD2 of 80-90 Gy is recommended [27, 28]. In our cohort, the median total EQD2 was 83 Gy, which was among the key factors influencing treatment response.

Perez and colleagues showed that prolonged overall treatment duration in 1224 cervical cancer patients receiving definitive RT was associated with reduced pelvic control and survival [29]. Krusun *et al.*, in a study of 107 cervical cancer patients treated with CRT, found that extended treatment duration adversely affected 3-year OS outcomes [30]. Our study also identified prolonged treatment duration as a key factor negatively influencing local control.

Similar to our findings, Lucia *et al.* and Leseur *et al.* reported that GLRLM-based features were significantly associated with survival and recurrence in cervical cancer patients.

Our findings align with previous radiomic studies that demonstrated the predictive value of GLRLM and GLZLM metrics in cervical cancer, while further emphasizing the role of treatment-related variables such as total EQD2 and therapy interruption duration.

This highlights the added prognostic relevance of integrating radiomic parameters with clinical and dosimetric factors to enhance individualized treatment prediction.

This study has several limitations, primarily its retrospective nature, single-institutional design, and modest sample size.Moreover, the absence of external validation reduces the generalizability of our findings. Nevertheless, our results support the prognostic value of radiomic features and provide a basis for future clinical research.

Our findings highlight the prognostic and predictive utility of radiomics in cervical cancer patients undergoing RT, in line with prior studies [31, 32].

In conclusion, radiomic analysis offers a valuable framework for constructing reliable predictive models that can refine patient stratification and guide truly individualized therapeutic decisions Integrating radiomics with clinical and dosimetric variables has the potential to improve oncologic outcomes while minimizing treatment-related adverse effects [33, 34].

Acknowledgments: There are no acknowledgments.

Conflict of Interest: The authors declare no conflicts of interest related to this work.

Funding: This research received no financial support from any governmental, commercial, or non-profit organization.

Ethical Consideration: The study protocol was approved by the Non-Interventional Clinical Research Ethics Committee of Eskişehir Osmangazi University (Approval No: E-25403353-050.04-240226745, Date: 28 November 2024).

Authors' contribution: Conceptualization: M.Y., D.E., K.D., E.G., E.C., and B.B. Data curation: M.Y., K.D., and B.B. Formal analysis: E.C. and E.G. Manuscript drafting: M.Y., D.E., K.D., E.G., E.C., and B.B. Critical review and editing: All authors read, revised, and approved the final version of the manuscript.

***AI usage in manuscript preparation*:** AI-based algorithms (kNN and MLP) were implemented for predictive modeling as a core component of the study's design and analysis.

REFERENCES

1. Bailey HH, Chuang LT, duPont NC, *et al.* (2016) American Society of Clinical Oncology statement: Human papillomavirus vaccination for cancer prevention. *J Clin Oncol, **34**: 1803-1812*.
2. Munoz N, Bosch FX, de Sanjose S and Shah KV (1994) The role of HPV in the etiology of cervical cancer. *Mutat Res, **305**: 293-301*.
3. Bray F, Loos AH, McCarron P, *et al.* (2005) Trends in cervical squamous cell carcinoma incidence in 13 European countries: changing risk and the effects of screening. *Cancer Epidemiol Biomarkers Prev, **14**: 677-686*.
4. Elmahdy M and Sebro R (2023) Radiomics analysis in medical imaging research. *J Med Radiat Sci, **70**: 3-7*.
5. Russo L, Charles-Davies D, Bottazzi S, Sala E and Boldrini L (2024) Radiomics for clinical decision support in radiation oncology. *Clin Oncol (R Coll Radiol), **36**: e269-e281*.
6. Xu H, Wang A, Zhang C, Ren J, Zhou P and Liu J (2023) Intra- and peritumoral MRI radiomics assisted in predicting radiochemotherapy response in metastatic cervical lymph nodes of nasopharyngeal cancer. *BMC Med Imaging, **23**: 66*.
7. Lin CH, Yan JL, Yap WK, *et al.* (2023) Prognostic value of interim CT-based peritumoral and intratumoral radiomics in laryngeal and hypopharyngeal cancer patients undergoing definitive radiotherapy. *Radiother Oncol, **189**: 109938*.
8. ClinicalTrials.gov (2015) Testing the addition of a new anti-cancer drug, triapine, to the usual chemotherapy treatment (cisplatin) during radiation therapy for advanced-stage cervical and vaginal cancers. NRG-GY006.
9. Lim K, Small W Jr, Portelance L, *et al.* Gyn IMRT Consortium (2011) Consensus guidelines for delineation of clinical target volume for intensity-modulated pelvic radiotherapy for the definitive treatment of cervix cancer. *Int J Radiat Oncol Biol Phys, **79**: 348-355*.
10. Chawla NV, Bowyer KW, Hall LO and Kegelmeyer WP (2002) SMOTE: synthetic minority over-sampling technique. *J Artif Intell Res, **16**: 321-357*.
11. Song C and Zhang H (2014) Comments on fifty years of classification and regression trees. *Int Stat Rev, **82**: 359-361*.
12. Goodfellow I, Bengio Y, Courville A (2016) Deep learning. MIT Press, Cambridge, MA, USA.
13. Manganaro L, Nicolino GM, Dolciami M, *et al.* (2021) Radiomics in cervical and endometrial cancer. *Br J Radiol, **94**: 20201314*.
14. Lubner MG, Smith AD, Sandrasegaran K, Sahani DV, Pickhardt PJ (2017) CT texture analysis: definitions, applications, biologic correlates, and challenges. *Radiographics, **37**: 1483-1503*.
15. Aerts HJ, Velazquez ER, Leijenaar RT, *et al.* (2014) Decoding tumour phenotype by noninvasive imaging using a quantitative radiomics approach. *Nat Commun, **5**: 4006*.
16. Zhang S, Regan K, Najera J, Grinstaff MW, Datta M and Nia HT (2023) The peritumor microenvironment: physics and immunity. *Trends Cancer, **9**: 609-623*.
17. Tang X (1998) Texture information in run-length matrices. *IEEE Trans Image Process, **7**: 1602-1609*.
18. Nioche C, Orlhac F, Boughdad S, *et al.* (2018) LIFEx: a freeware for radiomic feature calculation in multimodality imaging to accelerate advances in the characterization of tumor heterogeneity. *Cancer Res, **78**: 4786-4789*.
19. Olivares-Urbano MA, Griñán-Lisón C, Marchal JA, Núñez MI (2020) CSC radioresistance: a therapeutic challenge to improve radiotherapy effectiveness in cancer. *Cells, **9**: 1651*.
20. Jha AK, Mithun S, Sherkhane UB, *et al.* (2023) Development and validation of radiomic signature for predicting overall survival in advanced-stage cervical cancer. *Front Nucl Med, **3**: 1138552*.
21. Lucia F, Visvikis D, Desseroit MC, *et al.* (2018) Prediction of outcome using pretreatment 18F-FDG PET/CT and MRI radiomics in locally advanced cervical cancer treated with chemoradiotherapy. *Eur J Nucl Med Mol Imaging, **45**(5): 768-786*.
22. Leseur J, Roman-Jimenez G, Devillers A, *et al.* (2016) pre-and per-treatment 18F-FDG PET/CT parameters to predict recurrence and survival in cervical cancer. *Radiother Oncol, **120**(3): 512-518*.
23. Ferreira M, Lovinfosse P, Hermesse J, *et al.* (2021) [18F] FDG PET radiomics to predict disease-free survival in cervical cancer: a multi -scanner/center study with external validation. *Eur J Nucl Med Mol Imaging, **48**(11): 3432-3443*.
24. Liu B, Sun Z, Xu ZL, *et al.* (2022) Predicting disease-free survival with multiparametric MRI-derived radiomic signature in cervical cancer patients underwent CCRT. *Front Oncol, **11**: 812993*.
25. Liu D, Zhang X, Zheng T, *et al.* (2021) Optimisation and evaluation of the random forest model in the efficacy prediction of chemoradiotherapy for advanced cervical cancer based on radiomics signature from high-resolution T2 weighted images. *Arch Gynecol Obstet, **303**(3): 811-820*.
26. Ho KC, Fang YH, Chung HW, *et al.* (2016) A preliminary investigation into textural features of intratumoral metabolic heterogeneity in 18F-FDG PET for overall survival prognosis in patients with bulky cervical cancer treated with definitive concurrent chemoradiotherapy. *Am J Nucl Med Mol Imaging, **6**(3): 166-175*.
27. Dimopoulos JC, Lang S, Kirisits C, *et al.* (2009) Dose-volume histogram parameters and local tumor control in magnetic resonance image-guided cervical cancer brachytherapy. *Int J Radiat Oncol Biol Phys, **75**(1): 56-63*.
28. Dimopoulos JC, Pötter R, Lang S, *et al.* (2009) Dose-effect relationship for local control of cervical cancer by magnetic resonance image-guided brachytherapy. *Radiother Oncol, **93**(2): 311-315*.
29. Perez CA, Grigsby PW, Castro-Vita H, Lockett MA (1995) Carcinoma of the uterine cervix. I. Impact of prolongation of overall treatment time and timing of brachytherapy on outcome of radiation therapy. *Int J Radiat Oncol Biol Phys, **32**(5): 1275-1288*.
30. Krusun S, Pesee M, Supakalin N, Thamronganantasakul K, Supaadirek C, Padoongcharoen P (2014) Treatment interruption during concurrent chemoradiotherapy of uterine cervical cancer; analysis of factors and outcomes. *Asian Pac J Cancer Prev, **15**(14): 5653-5657*.
31. Sadati E, Hashemi B, Mahdavi SR, Nikoufar A, Abdollahi H (2025) Predicting prostate cancer radiotherapy complications: An integrated approach using radiomics, dosiomics, and machine learning. *Int J Radiat Res, **23**(1): 239-244*.
32. Cao S and Shu Z (2024) Spectral CT based radiomics for predicting brain metastases in patients with lung cancer. *Int J Radiat Res, **22** (2): 347-353*.
33. Cai Z, Li S, Xiong Z, Lin J, Sun Y (2024) Multimodal MRI-based deep-radiomics model predicts response in cervical cancer treated with neoadjuvant chemoradiotherapy. *Sci Rep, **14**(1): 19090*.
34. Jeong S, Yu H, Park SH, Woo D, Lee SJ, Chong GO, Han HS, Kim JC (2024) Comparing deep learning and handcrafted radiomics to predict chemoradiotherapy response for locally advanced cervical cancer using pretreatment MRI. *Sci Rep, **14**(1): 1180*.